Comparison of Mechanical Properties of PP/SEBS Blends at Intermediate and High Strain Rates with SiO_2 Nanoparticles Vs. $CaCO_3$ Fillers

Hiroyuki Mae,[1] Masaki Omiya,[2] Kikuo Kishimoto[3]

[1]*Honda R&D Co., Ltd., 4630 Shimotakanezawa, Haga-machi, Haga-gun, Tochigi 321-3393, Japan*
[2]*Department of Mechanical Engineering, Keio University, 3-14-1, Hiyoshi, Kohoku-ku, Yokohama-shi, Kanagawa, 223-8522, Japan*
[3]*Department of Mechanical and Sciences Engineering, Tokyo Institute of Technology, 2-12-1, O-okayama, Meguro, Tokyo, 152-8552, Japan*

Received 1 March 2008; accepted 15 May 2008
DOI 10.1002/app.28724
Published online 10 July 2008 in Wiley InterScience (www.interscience.wiley.com).

ABSTRACT: The present article focuses on the effect of two types of inorganic fillers (SiO_2 and $CaCO_3$) on the mechanical properties of PP/SEBS blend. The nominal particle diameters of SiO_2 and $CaCO_3$ are 7 nm and 1 μm, respectively. The studied blend ratios were PP/SEBS/SiO_2 ($CaCO_3$) = 75/22/3 and 73/21/6 vol %. The morphology of polymer blends was observed and the distributions of the SEBS, SiO_2, and $CaCO_3$ particles were analyzed by transmission electron microscopy (TEM). Tensile tests were conducted at nominal strain rates from 3×10^{-1} to 10^2 s^{-1}. The apparent elastic modulus has the local strain-rate dependency caused by SiO_2 nanoparticles around SEBS particles in the blend of PP/SEBS/SiO_2. The yield stress has weak dependency of morphology. The absorbed strain energy has strong dependency of the location of SiO_2 nanoparticle or $CaCO_3$ fillers and SEBS particle in the morphology. It is considered that such morphology, in which inorganic nanoparticles are located around SEBS particles, can prevent the brittle fracture while the increased local strain rate can enhance the apparent elastic modulus of the blend at the high strain rate. On the basis of the results of this study, the location and size of inorganic nanoparticles are the most important parameters to increase the elastic modulus without decreasing the material ductility of the blend at both low and high strain rates. © 2008 Wiley Periodicals, Inc. J Appl Polym Sci 110: 1145–1157, 2008

Key words: mechanical properties; morphology; crazing; poly(propylene) (PP); fillers

INTRODUCTION

The use of inorganic filler has become widespread for improving the mechanical properties of polymer blends.[1–31] The effects of inorganic filler on the mechanical properties of the composites depend strongly on their shape, particle size, aggregating size, surface characteristics, and the properties of the matrix. In addition, the filler dispersion and the matrix-particle bonding are also very important parameters for the toughening by inorganic fillers.

$CaCO_3$ is one of the most commonly used inorganic fillers in PP matrix. Xavier et al.[17] prepared the notched PP specimens with 40 wt % of $CaCO_3$ fillers and fractured at −30, 25, and 80°C. They showed that the incorporation of $CaCO_3$ avoided the catastrophic failure of PP at −30°C. Fekete et al.[18] evaluated the tensile mechanical properties of PP/$CaCO_3$ composites with different-size $CaCO_3$ fillers ranging from 0.08 to 12 μm. Their results showed that the particulate fillers aggregated when their particle size was smaller than a critical value. Then, the dominant fracture mechanism was the debonding between the fillers and PP matrix in the composites containing the relatively large fillers while that was the crack initiation inside the aggregation in the presence of extensive aggregation of small particles. Chan et al.[19] showed that $CaCO_3$ nanoparticles could act as stress concentration sites, which could promote cavitation at the particle–polymer boundaries during loading. This cavitation released the plastic constraints and triggered mass plastic deformation of the matrix, leading to much improved fracture toughness. Leong et al.[20] compared the mechanical properties of PP/$CaCO_3$, PP/talc, and PP/talc/$CaCO_3$ blends. A synergistic hybridization effect was observed in the flexural strength and impact strength in the blend (PP/talc/$CaCO_3$ = 70/15/15 wt %). In addition to the researches about the single-filler PP composites, there were many researches about the hybrid PP composite systems consisting of

Correspondence to: H. Mae (Hiroyuki_Mae@n.t.rd.honda.co.jp).

PP, elastomer, and $CaCO_3$ fillers. Maerinrri and Ricco[21] prepared two particulate hybrid systems containing of PP with particles of ethylene–propylene rubber (EPR) and $CaCO_3$. It was investigated that the hybridization of the secondary phase produced the optimization of the impact fracture properties compared with the corresponding binary systems. Premphet and Horanont[22] demonstrated the mechanical properties of PP/EOR (ethylene-octene copolymer)/$CaCO_3$ and PP/EVA (ethylene-vinyl acetate)/$CaCO_3$. Their results indicated the composites with separate dispersion of each phase showed higher modulus and impact strength than those of encapsulation type.

SiO_2 is another commonly used inorganic fillers in PP matrix as well. Many researches have been conducted on PP with SiO_2.[23–31] Rong et al.[23–26] demonstrated that the mechanical properties of PP could be effectively improved by the incorporation of a small amount of modified SiO_2 nanoparticles (typically less than 3 vol %), which was much lower than the content required by the conventional particulate composites. Wu et al.[27] improved the tensile performance by adding SiO_2 nanoparticles into PP at filler content as low as 0.5 vol %. There are some limited researches for toughening PP blends with rubber by SiO_2 nanoparticles.[28–31] Lehmann et al.[28] demonstrated that a combination of the grafted SiO_2 nanoparticles and elastomeric modifier was able to significantly increase the toughness of PP including the notch impact resistance although pregrafted nano-SiO_2 particles were not good enough to reduce the notch sensitivity of PP. Yang et al.[29,30] studied the phase structures and toughening mechanism in PP/EPDM (ethylene–propylene–diene monomer rubber)/SiO_2 composites. They blended hydrophilic SiO_2 nanoparticles with PP/EPDM composite by using two-step processing method, leading to a unique phase structure that EPDM particles are closely surrounded by nano-SiO_2 particles. This unique microstructure enhanced the Izod impact strength because the stress fields overlapped between EPDM and SiO_2 particles.

In the previous study, the same authors characterized the effect of SiO_2 nanoparticles on the mechanical properties of PP/SEBS blended with two types of SEBS particles whose particle diameters were different at the intermediate and high strain rates.[31] On the basis of the results of the previous study, the location of SiO_2 nanoparticles is the most important parameters to increase the elastic modulus without decreasing the material ductility in the blend (PP/SEBS/SiO_2) at both low and high strain rates. However, the previous study focused only on the large and small size SEBS particles with a fixed volume of SiO_2 nanoparticles. Thus, it is interesting to investigate the effect of volume ratio of SiO_2 nanoparticles on the mechanical properties of PP/SEBS/SiO_2 blend.

In addition, the studies about the effects of different inorganic filler's particle sizes on the material ductility in PP blended with SEBS at the intermediate and high strain rates are very limited. Therefore, the present article focuses on the effect of two types of inorganic fillers (SiO_2 and $CaCO_3$) on the mechanical properties of PP/SEBS blend. The nominal particle diameters of SiO_2 and $CaCO_3$ are 7 nm and 1 μm, respectively. The studied blend ratios for SiO_2 were PP/SEBS/SiO_2 = 75/22/3 and 73/21/6 vol % while those for $CaCO_3$ were PP/SEBS/$CaCO_3$ = 75/22/3 and 73/21/6 vol %. The morphology of polymer blends was observed and the distribution sizes of the SEBS particles, SiO_2 and $CaCO_3$ were analyzed by transmission electron microscopy (TEM). Tensile tests were conducted at nominal strain rates from 3×10^{-1} to 10^2 s^{-1}. The difference of toughening mechanisms between PP/SEBS/SiO_2 and PP/SEBS/$CaCO_3$ was discussed. In addition, the microstructural finite element (FE) analysis was conducted to investigate the craze growth, the stress triaxiality and the local strain rate at the microscopic level.

EXPERIMENTAL

Materials

Isotactic polypropylene (i-PP: J-3003GV, Prime Polymer, Japan) whose molecular weight Mn was about 33,000 was used as the matrix polymer in this study. It has a melt flow rate (MFR) = 30 g/10 min (230°C). The density of i-PP was 900 kg/m^3. The styrene-ethylene-butadiene-styrene triblock copolymers (SEBS) (H1062), Asahi Kasei Chemicals, Japan), was used. According to the supplier's technical data sheet, the MFR is 4.5 (g/10 min at 230°C) and the weight ratio of stylene/ethylene-butylene is 18/82 wt %. The SiO_2 inorganic filler was hydrophilic SiO_2 nanoparticle (Aerosil 300, Nippon Aerosil, Japan) whose density was about 2200 kg/m^3. The $CaCO_3$ inorganic filler was hydrophilic $CaCO_3$ filler (PO-320-B-10, Shiraishi Calcium, Japan) whose density was about 2780 kg/m^3. The mean diameters of SiO_2 nanoparticle $CaCO_3$ filler were about 7 nm and 1 μm based on the technical data from the suppliers.

Blending and sample preparation

PP, SEBS copolymers, and SiO_2 (or $CaCO_3$) were melt-mixed in a corotating twin screw extruder (Berstorff, ZE40A), with a screw length of 1340 mm and a screw diameter of 40 mm. The temperature profile was controlled at 180°C (from feed to 800 mm), 186°C (from 800 to 1280 mm), 190°C (from 1280 to 1310 mm) and 192°C from 1310 to 1340 mm (die

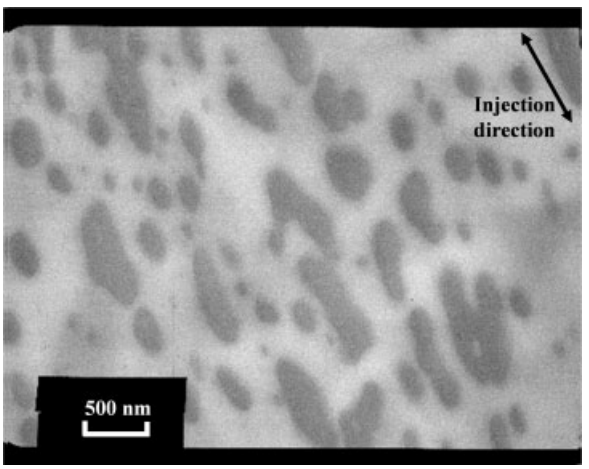

Figure 1 TEM morphological picture of PP/SEBS blend.

zones). The screw rotating speed was kept constant at 200 rpm. To make PP/SEBS/SiO_2 (or $CaCO_3$) blends, SEBS and SiO_2 (or $CaCO_3$) were melt-mixed, firstly. After that, PP and SEBS + SiO_2 (or $CaCO_3$) were melt-mixed at the same condition as the case of SEBS and PP. The blend ratio between PP and SEBS were 75/25 vol % in the PP/SEBS blend while the blend ratios of PP/SEBS/SiO_2 (or $CaCO_3$) were 75/22/3 and 73/21/6 vol %. Polypropylene toughened by rubber particles usually has about 20–30 vol % rubber for automotive applications. Then, the mechanical properties of PPs blended with wide range of SEBS contents were characterized by the same authors.[32–34] After melt-mixing process, the hot extrudate was immediately quenched in a water bath and palletized. All blends were prepared under the same conditions. The blends were injection-molded to the rectangular plate whose geometry was 150 × 150 × 3 mm^3. Finally, all tensile test specimens were cut out from the plates such that the tensile direction was the same as the injection direction.

Tensile test

ASTM dumbbell shape (parallel portion width 4.8 mm) microtensile test specimens are used for measuring the stress–strain relationship (ASTM D 1708). The thickness of test specimen is 3.0 mm. This study uses a servo-hydraulic high-speed impact test apparatus (Shimazu EHF U2H-20L: maximum tensile speed 15 m/s) to obtain mechanical characteristics under medium to high speed deformation. The nominal strain and nominal strain rate were calculated from the clamping distance of the test specimen where the gauge length was 22.2 mm. The nominal strain rate ranges from 3×10^{-1} to 10^2 s^{-1}. Fracture surface was observed by scanning electron microscopy (SEM: HITACHI *S*-4300SE/N).

Morphological investigation by TEM

Transmission electron microscope (TEM: JEOL JEM-200CX) operating at 160 keV was used to observe the phase morphology. After staining of samples with OsO_4, ultra-thin sections were sliced by ultra microtome equipped with diamond knife. The samples were taken from the parallel portion of the tensile specimen.

Figure 1 shows the morphology of the representative PP/SEBS blend where a two-phase morphology is clearly seen. SEBS particles are dispersed randomly in the PP matrix. The mean approximate diameters of SEBS were 180 nm based on the image analysis. In the image analysis, the commercial based software (Azo-kun, Asahi Kasei Engineering, Japan) was used. The rubber particles were approximated as a circle and then the diameter of each circle was collected manually in the software. The mean diameter of SEBS was quite similar to that obtained in the previous researches.[32,33]

Figure 2 shows the morphologies of PP/SEBS/SiO_2 and PP/SEBS/$CaCO_3$ composites, respectively. In the morphological pictures, the white and black regions correspond to PP and SEBS phases, respectively. In addition, the gray-color region means SiO_2 and $CaCO_3$ phases in each blend. In Figure 2(c and d), $CaCO_3$ particles are identified by the black-color circles. $CaCO_3$ particles will be also shown in the SEM pictures of the fracture surfaces at the nominal strain rate of 100 s^{-1}. As shown clearly, SiO_2 nanoparticles are dispersed randomly in PP matrix with the aggregation of SiO_2 particles while $CaCO_3$ fillers are randomly dispersed without aggregation. It is clear that the diameter of SiO_2 aggregation in PP/SEBS/SiO_2 composite was smaller than the diameter of $CaCO_3$ fillers in PP/SEBS/$CaCO_3$ blend. In the blend (PP/SEBS/SiO_2), it seems that SiO_2 particles aggregated along the boundary between SEBS particle and PP matrix because the outlines of particles in PP matrix had many corners as shown in Figure 2. On the basis of the image analysis, the mean approximate diameters of SiO_2 aggregates with SEBS particles was 430 nm. Clearly, the size of SiO_2 aggregation was much larger than that of SEBS particle of PP/SEBS blend. On the contrary, $CaCO_3$ were well dispersed in PP/SEBS matrix.

NUMERICAL PROCEDURE

To investigate stress distributions, craze nucleation and growth around SEBS particles and SiO_2/$CaCO_3$ fillers, finite element (FE) analyses were carried out by developing the plane strain microstructural model based on the morphological TEM pictures. Figure 3 shows the microstructural FE models developed by using OOF software[35] with the boundary conditions in the blends of PP/SEBS/SiO_2 ($CaCO_3$)

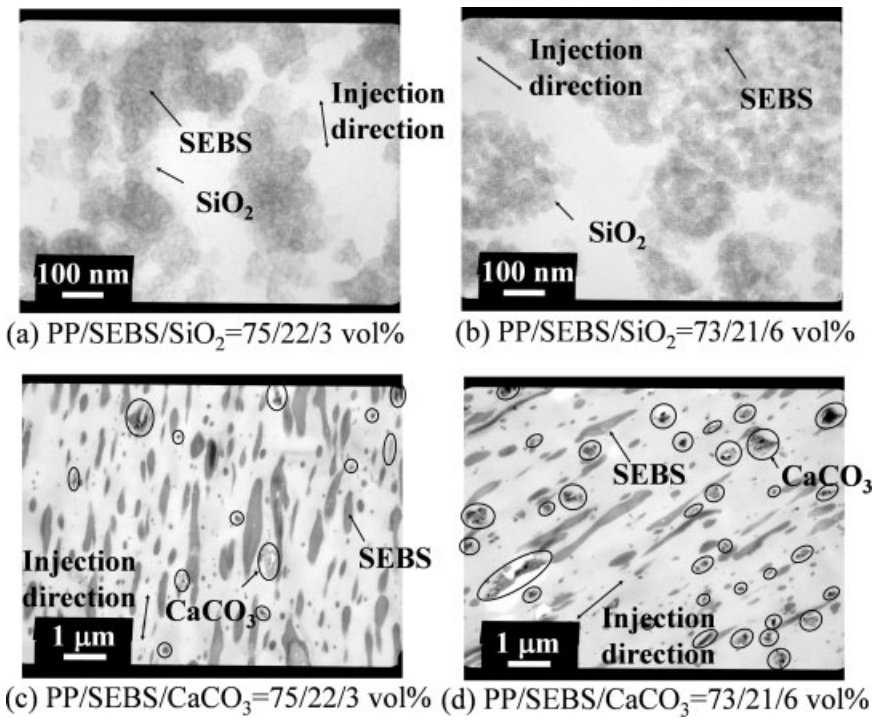

Figure 2 TEM morphological pictures of various blends.

= 75/22/3 and 73/21/6 vol %. The left-hand side was constrained for their horizontal movements and the bottom side was fixed for its vertical movement. The enforced displacement was applied on the right-hand side and the upper side. The applied strain rate corresponded to 100 s^{-1} in each direction. Finite element analyses were carried out by using the general explicit solver, RADIOSS version 4.4 with the user defined material subroutine program developed for predicting the craze nucleation and growth.[36–39] RADIOSS is a comprehensive transient, dynamic finite element solver to simulate impact, safety-related performance, manufacturing processes and fluid-structure interaction problems.

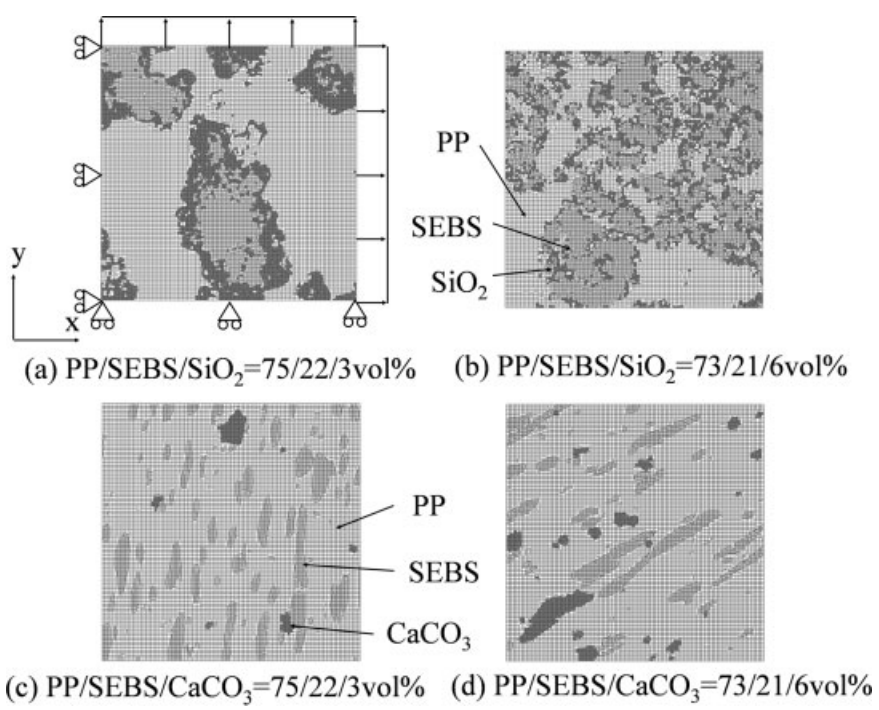

Figure 3 Microstructural FE models.

TABLE I
Material Coefficients for Finite Element Analysis with Elastic Modulus E = 800 MPa and Poisson's Ratio μ = 0.41

A	0.192
B	0.613
A_1	1.982 (MPa)
B_1	417.665 (MPa·MPa)
D_1	0.999
D_2	100.541
ε_c	1.087
m	0.069
$\dot{\varepsilon}_r$	1 (s^{-1})
σ_r	10.055 (MPa)
σ_y	17.432 (MPa)
k_1	44.795
k_2	0.863
k_3	1.243
q_1	0.0001177
q_2	12.44
q_3	2.908
σ_r	0.0001

The proposed elastoviscoplastic constitutive equation with craze effect is shown as eq. (1)[36,37];

$$\overset{\nabla}{\mathbf{T}} = \mathbf{C}^{v} : \mathbf{D} - \dot{\bar{\varepsilon}}^{p}(\cos\,\delta)\mathbf{P}' - \dot{\omega}\mathbf{T}/(1-\omega), \quad (1)$$

where $\mathbf{T}$ is Cauchy stress, $\mathbf{D}$ is deformation rate, $\dot{\bar{\varepsilon}}^{p}$ is equivalent plastic strain rate, ω is craze density, $\dot{\omega}$ is craze density rate, and $(\overset{\nabla}{})$ is Jaumann rate. $\mathbf{C}^{v}$, $\mathbf{P}'$, and cos δ are defined in the following equations:

$$\mathbf{C}^{v} \equiv H_{\omega}(1-\omega)/(H_{\omega}+3\mu)[\mathbf{C}^{e}+3\mu/H \times\{(3\lambda+2\mu)/3\mathbf{I}\otimes\mathbf{I}+3\mu\mathbf{T}'\otimes\mathbf{T}'/\bar{\sigma}^{2}\}] \quad (2)$$

$$\mathbf{P}' \equiv \mathbf{C}^{v} : \mathbf{m}' = 3\mu(1-\omega)\mathbf{T}'/\bar{\sigma}, \quad \mathbf{m}' \equiv 3/2\mathbf{T}'/\bar{\sigma}, \quad (3)$$

$$H_{\omega} \equiv 1/(1-\omega)\bar{\dot{\sigma}}/(\dot{\bar{\varepsilon}}^{p}k), \quad \bar{\dot{\sigma}} \equiv (3\overset{\nabla}{\mathbf{T}}'\cdot\overset{\nabla}{\mathbf{T}}'/2)^{1/2}, \quad (4)$$

$$\cos\,\delta = (1-\sin^{2}\,\delta)^{1/2}, \quad \sin\,\delta = k(m)\sin\,\alpha, \quad (5)$$

where $\mathbf{m}'$ is stress direction tensor, m is the strain rate sensitivity parameter and cos α is defined as

$$\cos\,\alpha \equiv \mathbf{T}'\cdot\overset{\nabla}{\mathbf{T}}'(\mathbf{T}'\cdot\mathbf{T}')^{-1/2}(\overset{\nabla}{\mathbf{T}}'\cdot\overset{\nabla}{\mathbf{T}}')^{-1/2}. \quad (6)$$

The craze evolution equation is proposed in the following equation;[38]

$$\dot{\omega} = A(1-\omega)\langle\dot{\varepsilon}_{m}^{p}\rangle + 1/2\;BD_1^{\bar{\varepsilon}^{p}}[1+\tanh\{-D_2(\bar{\varepsilon}^{p}-\varepsilon_c)\}]\dot{\bar{\varepsilon}}^{p}, \quad (7)$$

where A, B, D_1, and D_2 are material constants. $\dot{\varepsilon}_{m}^{p}$ is the mean normal plastic strain rate and is defined as

$$\dot{\varepsilon}_{m}^{p} = \{(q_1\omega)\cosh\big((q_2\omega+q_3)\sigma_m/\sigma_y\big)\}^{\bullet}, \quad (8)$$

where σ_m is the hydrostatic stress, σ_y is the yield stress, q_1–q_3 are material constants. The first part of eq. (7) means craze evolution and the second one means the craze creation and growth. ε_c is the strain at which the craze stops growing. The craze generation is based on the hydrostatic stress criterion as eq. (9);

$$\sigma_b \geq A_1 + (B_1/3\sigma_m) \qquad \sigma_b = \sigma_1 - \nu\sigma_2 - \nu\sigma_3, \quad (9)$$

in which σ_b is the stress needed for fibril orientation, σ_m is the hydrostatic stress, σ_1–σ_3 are the principal stresses, A_1 and B_1 are material constants.

With strain rate dependent coefficient m, the strain hardening equation is modeled in the following equations;

$$\dot{\bar{\varepsilon}}^{p} = \dot{\varepsilon}_r|\bar{\sigma}/g(\bar{\varepsilon}^{p})|^{1/m}, \quad (10)$$

$$g(\bar{\varepsilon}^{p}) = \sigma_r\{\tanh(k_1\bar{\varepsilon}^{p}) + k_2 + H_e(\bar{\varepsilon}^{p}-\varepsilon_r)k_3(\exp\,\bar{\varepsilon}^{p} - \exp\,\varepsilon_r)\}, \quad (11)$$

where $g(\bar{\varepsilon}^{p})$ is the flow stress modeled for polypropylene, $\dot{\varepsilon}_r$ is the reference strain rate, σ_r is the reference stress, ε_r is the reference strain at which the second hardening begins. k_1–k_3 are material constants. $H_e(x)$ is the following step function.

$$H_e(x) = 1 \quad (\text{at } x > 0), \quad 0\;(\text{at } x < 0). \quad (12)$$

The material properties of PP matrix were identified by the same authors in the previous study as shown in Table I.[39] This numerical procedure was successfully applied to the microstructural FE models in the previous study.[34] SEBS particles, SiO_2 and $CaCO_3$ were assumed to be elastic materials for simplicity. Young's modulus and Poisson's ratio for SEBS were 1.4 MPa and 0.499. Those of SiO_2 and $CaCO_3$ were 80 GPa and 0.17.

RESULTS AND DISCUSSION

Tensile mechanical properties of PP/SEBS, PP/SEBS/SiO_2 and PP/SEBS/$CaCO_3$ blends

Tensile tests under each condition were conducted three times. The typical stress strain curves at the strain rate of 10 s^{-1} are shown in Figure 4. It is shown that the stress reduction of the blend (PP/SEBS) is the smallest among all other blends. It is expected that the craze growth is different among all blends because the yield stresses are almost the same. The interesting result here is that the rupture strain of PP/SEBS/SiO_2 blend decreased drastically as the volume ratio of SiO_2 increased. On the contrary, the

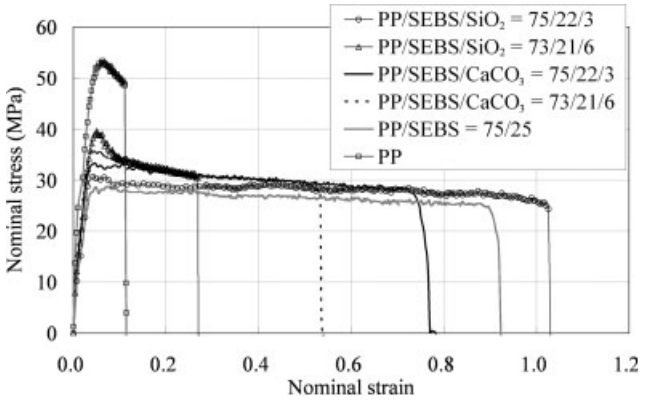

Figure 4 Typical stress strain curves at the nominal strain rate of 10 s^{-1}.

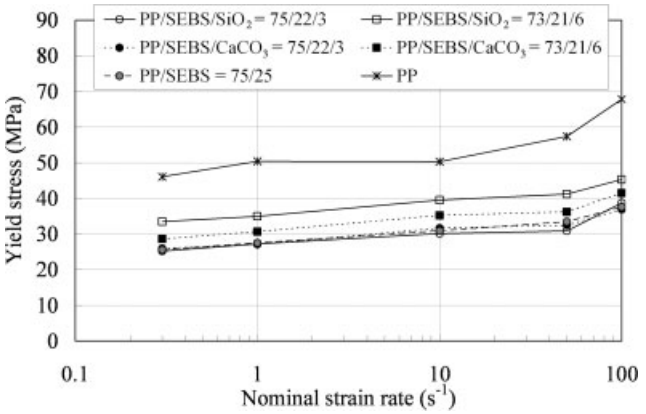

Figure 6 Effect of strain rate on yield stress in various blends.

difference of the rupture strain among PP/SEBS/$CaCO_3$ blends was small. The flow stress of neat PP is about twice as large as those of PP/SEBS/SiO_2 and PP/SEBS/$CaCO_3$ blends while the rupture strain of neat PP is the smallest among all blends.

Figure 5 shows the mean apparent elastic moduli calculated from three measurement data. As shown clearly, the elastic modulus increased when the nominal strain rate increased in all blends. It is expected that the ductile brittle transition would occur at the nominal strain rate between 10 and 100 s^{-1} in all blends. The apparent elastic moduli of PP/SEBS/SiO_2 and PP/SEBS/$CaCO_3$ blends were about half as large as that of neat PP at the nominal strain rates below 10 s^{-1} while they were similar to the apparent elastic modulus of the PP/SEBS blend. On the contrary, at the nominal strain rates above 50 s^{-1}, it appeared that the difference of the apparent elastic moduli between the PP/SEBS/SiO_2 and PP/SEBS/$CaCO_3$ blends became large. For example, the apparent elastic moduli of PP/SEBS/SiO_2 were larger than PP/SEBS by about 30% although those of the PP/SEBS/$CaCO_3$ were similar to the PP/SEBS blend at the nominal strain rate of 100 s^{-1}, as shown in Figure 5. It is considered that the morphological difference should have large effects on those differences. As shown in TEM morphological pictures, a number of SiO_2 particles were distributed around SEBS particles in the PP/SEBS/SiO_2 blends while $CaCO_3$ fillers were separately located in the PP matrix of the blends (PP/SEBS/$CaCO_3$). The similar trend was obtained in the molecular dynamics study.[40,41] It is considered that the same stiffening mechanism would work in the PP/SEBS/SiO_2 blends.

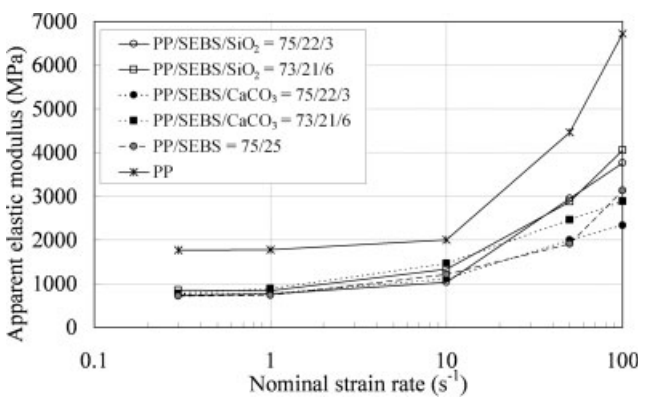

Figure 5 Effect of strain rate on elastic modulus in various blends.

The yield stress was defined as the maximum nominal stress. In the same manner as the measurements of elastic modulus, the yield stress was measured three times at each condition, and the mean value is plotted in Figure 6. On the contrary to Figure 5, the yield stress shows the weak dependency of strain rate. In addition, the yield stress of neat PP was twice as large as those of all the blends (PP/SEBS/$CaCO_3$). However, the yield stress of the blends (PP/SEBS/SiO_2) increased as the volume ratio of SiO_2 increased. It is expected that the many SiO_2 nanoparticles dispersed directly in PP matrix enhanced the yield stress in the same manner as the apparent elastic modulus.

Figure 7 shows the mean rupture strain plotted against the nominal strain rate. Figure 8 shows the strain energy up to failure. The trend was similar between Figures 7 and 8. As shown clearly, the rupture strain and the strain energy up to failure had the strong dependency on the strain rate. As the nominal strain rate increased, the material ductility decreased in almost all blends. In the blend (PP/SEBS/SiO_2 = 73/21/6 vol %), the rupture strains were similar between the nominal strain rates of 0.3 and 100 s^{-1}. The fracture surfaces showed the brittle fracture at both strain rates, leading to the similar rupture strain in this blend. The interesting point here is that the rupture strain and strain energy up to failure decreased drastically by increasing SiO_2 nanoparticle in PP/SEBS/SiO_2 blend while those did not decrease drastically in PP/SEBS/$CaCO_3$ blends.

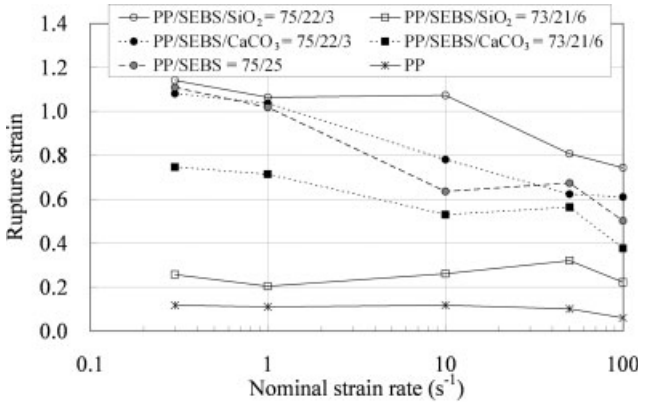

Figure 7 Effect of strain rate on rupture strain in various blends.

For example, the rupture strain and strain energy up to failure of the blend (PP/SEBS/SiO_2 = 73/21/6 vol %) are about one tenth as large as those of the blend (PP/SEBS/SiO_2 = 75/22/3 vol %) at the whole range of strain rates. On the contrary to the blends (PP/SEBS/SiO_2), the rupture strain and strain energy up to failure were kept similar even if $CaCO_3$ fillers were blended in PP/SEBS blend by 6 vol %. It is considered that the local damage process, such as craze nucleation and growth, is different among these blends. In PP/SEBS/SiO_2 blend, many SiO_2 aggregations dispersed directly in PP matrix, leading to high stress concentration at the interface between SiO_2 and PP matrix and inducing the bonding of SiO_2 particles from the PP matrix before the cavitation of SEBS particles. As a result, the toughening mechanism of SEBS particles did not work well and, hence, the rupture strain of the blend (PP/SEBS/SiO_2 = 73/21/6 vol %) decreased drastically about one tenth of the blend (PP/SEBS/SiO_2 = 75/22/3 vol %). In addition, it is considered that SiO_2 nanoparticles out of SEBS particles would have much larger interfacial area with PP matrix, compared with $CaCO_3$ fillers. SiO_2 nanoparticles have much larger relative area than $CaCO_3$ fillers because the nominal particle diameters are quite different. According to the technical data from the suppliers, the relative areas of SiO_2 and $CaCO_3$ are approximately 300 and 3.2 m^2/g, respectively. Even if the volume ratio of $CaCO_3$ fillers is same as that of SiO_2 nanoparticles, the difference of the interfacial area with PP matrix could be about 100 times between them.

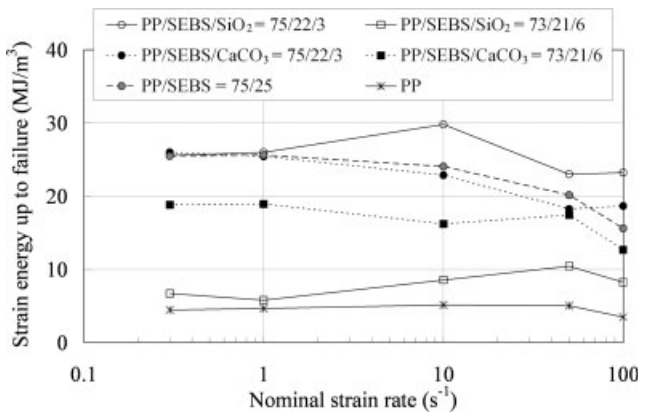

Figure 8 Effect of strain rate on strain energy up to failure in various blends.

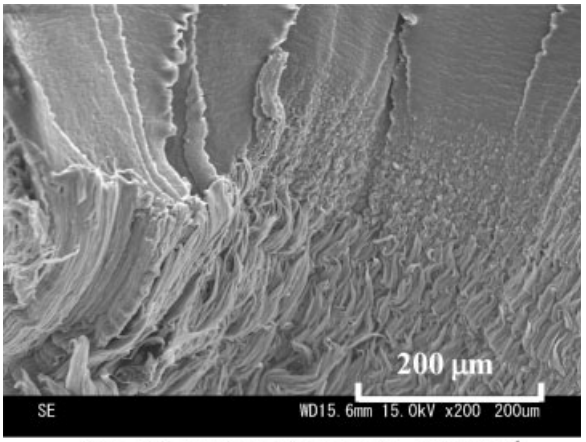

(a) At nominal strain rate of 0.3 s^{-1}

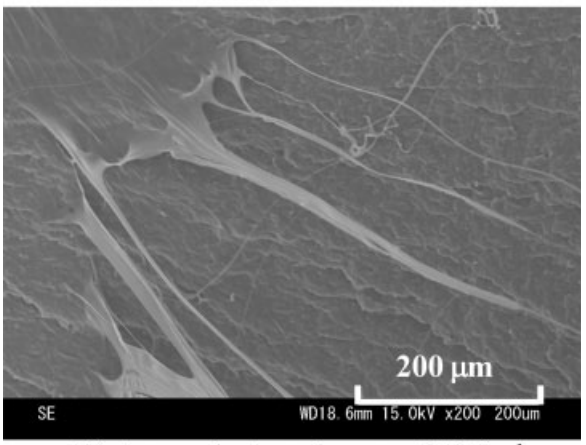

(b) At nominal strain rate of 100 s^{-1}

Figure 9 SEM pictures of fracture surfaces of PP/SEBS blend at the nominal strain rates of 0.3 and 100 s^{-1}.

SEM observation of fracture surfaces

The fracture surfaces at the nominal strain rate of 0.3 and 100 s^{-1} are shown in Figures 9–12. Figure 9 shows the fracture surfaces of PP/SEBS at the nominal strain rates of 0.3 and 100 s^{-1}, respectively. As shown clearly, the ductile fracture was the dominant mechanism in PP/SEBS blend at both low and high strain rates. Shear bands and crazes can be observed in Figure 9. Figure 10 shows the fracture surfaces of PP/SEBS/SiO_2 blends at the nominal strain rates of 0.3 and 100 s^{-1}. In the blend (PP/SEBS/SiO_2 = 75/22/3 vol %), the craze was observed in the nominal strain rate of 0.3 s^{-1} and the

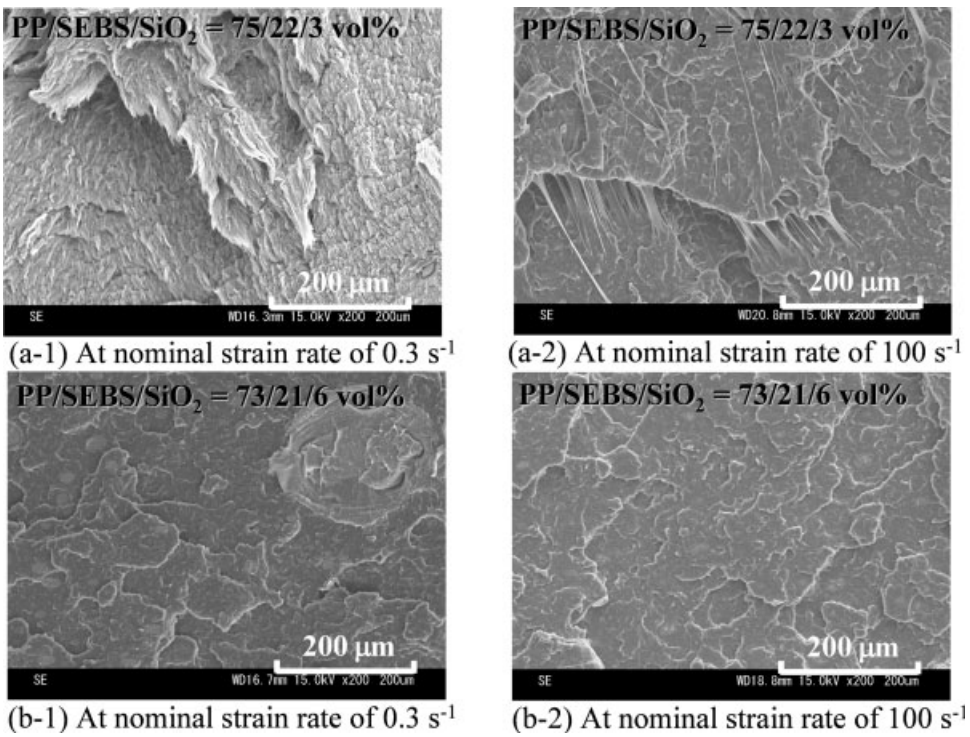

Figure 10 SEM pictures of fracture surfaces of PP/SEBS/SiO_2 blend at the nominal strain rates of 0.3 and 100 s^{-1}.

fibril was observed at the nominal strain rate of 100 s^{-1}. On the contrary, the smooth fracture surfaces were obtained in the blend (PP/SEBS/SiO_2 = 73/21/6 vol %) as shown in Figure 11 (b1 and b2).

Figure 11 shows the fracture surfaces of PP/SEBS/$CaCO_3$ blends at the nominal strain rates of 0.3 and 100 s^{-1}. In all blends (PP/SEBS/$CaCO_3$), the ductile fracture was the dominant fracture

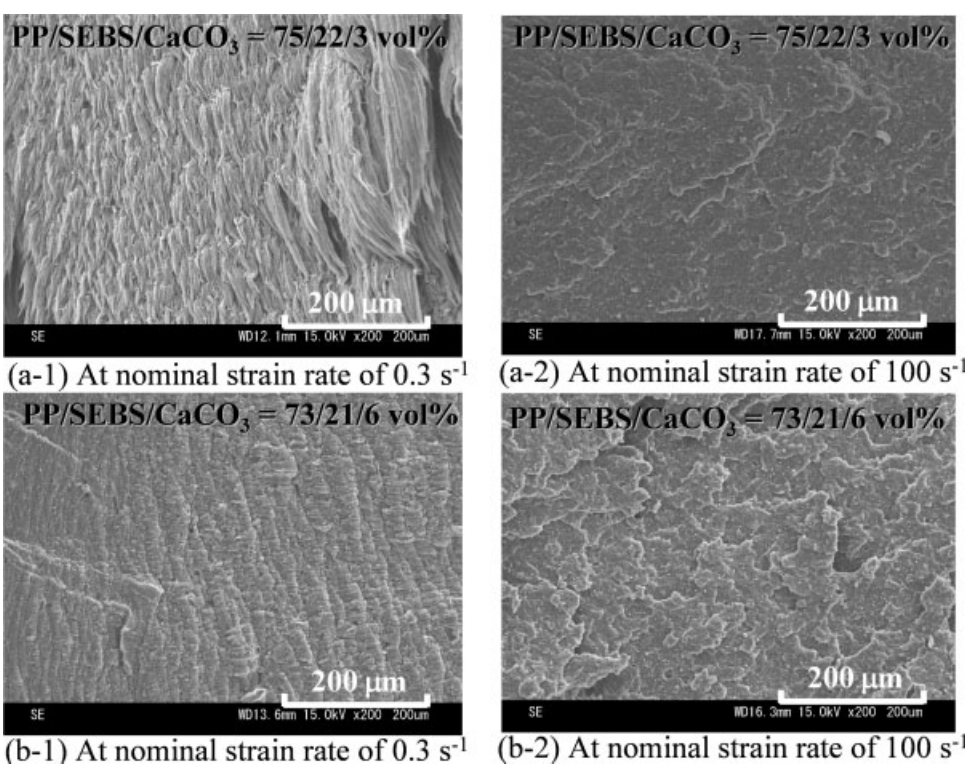

Figure 11 SEM pictures of fracture surfaces of PP/SEBS/$CaCO_3$ blends at the nominal strain rates of 0.3 and 100 s^{-1}.

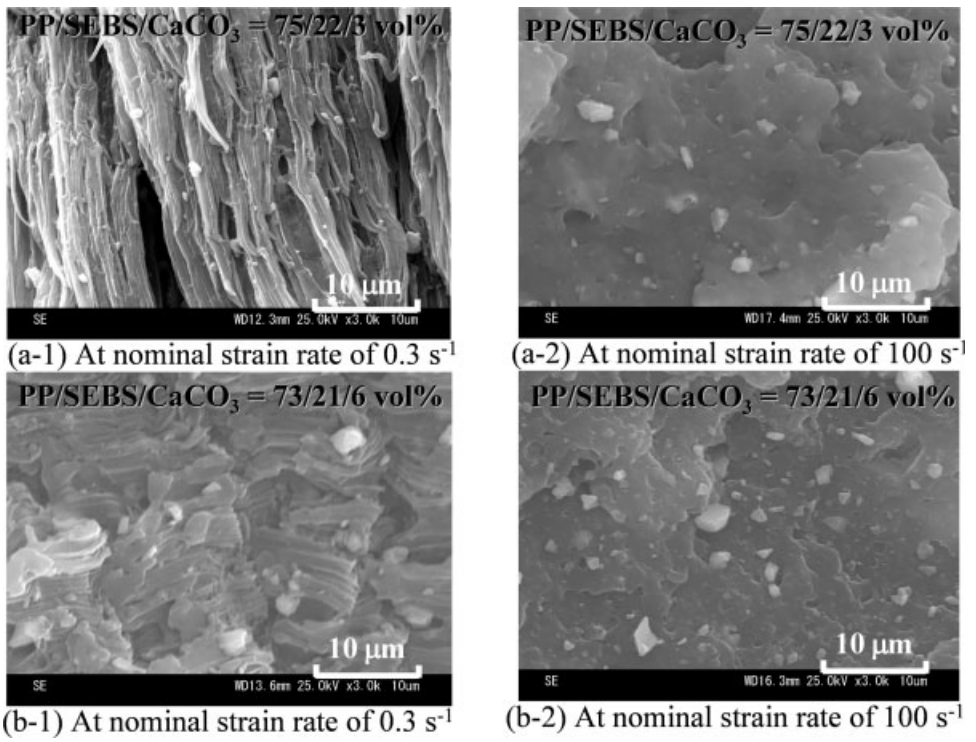

Figure 12 Magnified SEM pictures of fracture surfaces of PP/SEBS/$CaCO_3$ blends at the nominal strain rates of 0.3 and 100 s^{-1}.

mechanism at the nominal strain rate of 0.3 s^{-1} while the brittle fracture surfaces were observed at the nominal strain rate of 100 s^{-1} as shown in Figure 11. As the amount of $CaCO_3$ fillers increased, less fibrils were observed on the fracture surfaces. Figure 12 shows the magnified pictures of the fracture surfaces. The $CaCO_3$ fillers were observed on the fracture surfaces. At the nominal strain rate of 0.3 s^{-1}, $CaCO_3$ fillers were observed in the fibrillated crazes. In addition, the fibrils were split in the blends (PP/SEBS/$CaCO_3$ = 73/21/6 vol %) while the fibrils were highly elongated in the blend (PP/SEBS/$CaCO_3$ = 75/22/3 vol %). It is considered that the fibrils could not be highly elongated because the amount of SEBS particles decreased and $CaCO_3$ fillers increased. At the nominal strain rate of 100 s^{-1}, the brittle fracture surfaces with $CaCO_3$ fillers were observed in all the blends (PP/SEBS/$CaCO_3$).

Summary of mechanical properties

As a summary of the obtained mechanical properties, the elastic modulus and the strain energy up to failure were normalized by those of neat PP. The elastic modulus and the strain energy up to failure at the nominal strain rates below 10 s^{-1} were normalized by the mean elastic modulus and the mean strain energy of neat PP obtained at the nominal strain rate of 10 s^{-1}. Those at the nominal strain rates above 50 s^{-1} were normalized by the mean elastic modulus and the mean strain energy up to failure of neat PP obtained at the nominal strain rate of 100 s^{-1}. Figure 13 shows the relative elastic modulus plotted against the relative strain energy up to failure at the nominal strain rates below 10 s^{-1}. As shown clearly, the neat PP has the largest elastic modulus among them although the strain energy up to failure was the smallest. In the blends (PP/SEBS = 75/25 and PP/SEBS/SiO_2 = 75/22/3 vol %), both the elastic modulus and the strain energy up to failure were almost the same between them, which meant that SiO_2 nanoparticles did not decrease the strain energy up to failure in this particular blend.

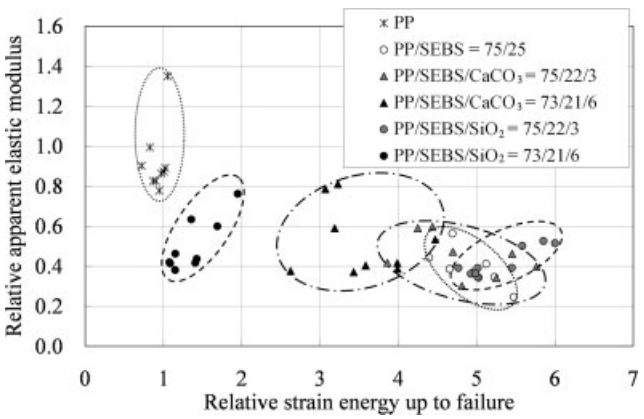

Figure 13 Relative elastic modulus plotted against the relative strain energy up to failure at the nominal strain rates below 10 s^{-1}.

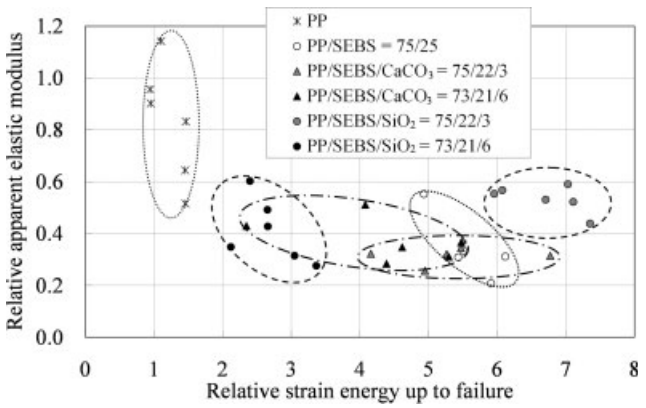

Figure 14 Relative elastic modulus plotted against the relative strain energy up to failure at the nominal strain rates above 50 s^{-1}.

On the contrary, in the blends (PP/SEBS/SiO_2 = 73/21/6 vol %), SiO_2 nanoparticles enhanced the elastic modulus while they decreased the strain energy up to failure. In all the blends (PP/SEBS/$CaCO_3$), $CaCO_3$ increased the elastic modulus with the decrease of strain energy up to failure. The interesting result here is that the decrease of the strain energy up to failure by blending SiO_2 nanoparticles was much larger than that by $CaCO_3$ fillers. Again, it is considered that the increase of the interfacial area by adding SiO_2 nanoparticles was much larger than that of $CaCO_3$ fillers because of the large difference of the particles size, leading to the ductile brittle transition.

Figure 14 shows the relative elastic modulus plotted against the relative strain energy up to failure at the nominal strain rates above 50 s^{-1}. The same trends of elastic moduli and strain energy up to failure were obtained in neat PP and the blends (PP/SEBS, PP/SEBS/SiO_2 and PP/SEBS/$CaCO_3$) as those obtained at the nominal strain rates below 10 s^{-1}. The interesting result here is that SiO_2 nanoparticles enhanced the elastic modulus without decreasing the strain energy up to failure in only the blend (PP/SEBS/SiO_2 = 75/22/3 vol %) as shown clearly in Figure 14. The mean apparent elastic modulus of this blend was 1.6 times as large as that of the blend (PP/SEBS = 75/25 vol %) at the nominal strain rate above 50 s^{-1} although they were almost the same at the nominal strain rate below 10 s^{-1}. The reason why SiO_2 enhanced the stiffness of this particular blend at the high strain rate would be such a unique morphology that the SiO_2 nanoparticles were located along the SEBS particles as shown in Figure 2. This unique morphology increased the local strain rate in the PP matrix, leading to the increase of the apparent elastic modulus at the nominal strain rates above 50 s^{-1}. The mean strain energy up to failure of the blend (PP/SEBS/SiO_2 = 75/22/3 vol %) increased by 20%, compared with that of the blend (PP/SEBS = 75/25 vol %). It is considered that SiO_2 nanoparticles around SEBS particles would be released during the large deformation, leading to the similar material ductility to the PP/SEBS blend. Thus, the location of the SiO_2 nanoparticles is important parameter for increasing the elastic modulus without decreasing the material ductility in the blend (PP/SEBS/SiO_2) at both low and high strain rates. Therefore, it would be necessary to study

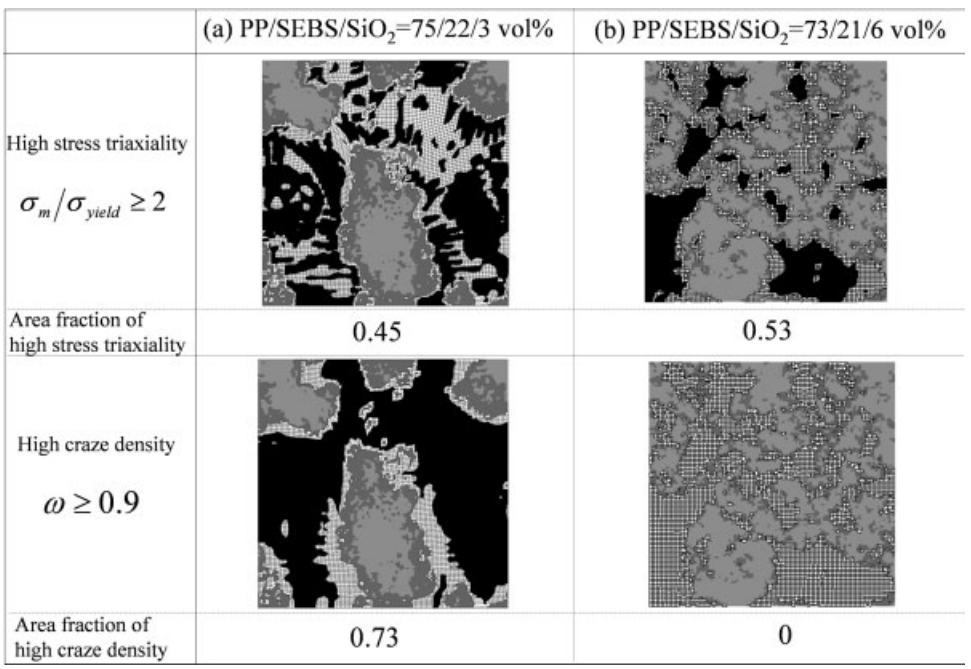

Figure 15 Simulated stress triaxiality and craze density distributions of PP/SEBS/SiO_2 blends at $\varepsilon_x = \varepsilon_y = 0.1$.

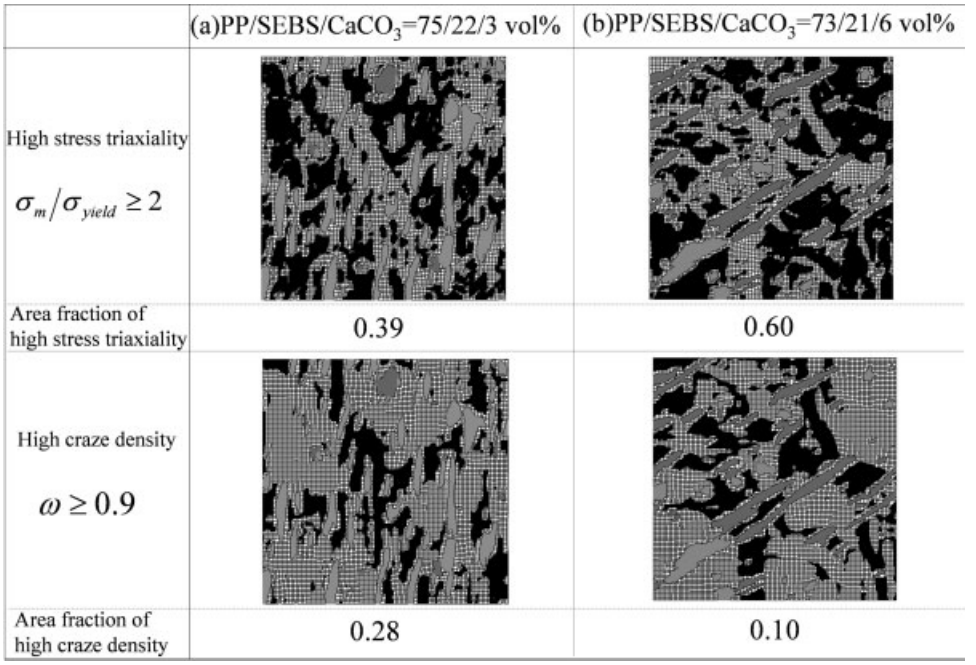

Figure 16 Simulated stress triaxiality and craze density distributions of PP/SEBS/$CaCO_3$ blends at $\varepsilon_x = \varepsilon_y = 0.1$.

further the effect of such a morphology on the elastic modulus and the ductility of the blend which is discussed in the next section.

Numerical results

Figures 15 and 16 show the distributions of stress triaxiality and craze density of PP/SEBS/SiO_2 ($CaCO_3$) blends at $\varepsilon_x = \varepsilon_y = 0.1$. As shown clearly, the craze density of the blend (75/22/3 vol %) was larger than that of the blend (73/21/6 vol %) in both blends (PP/SEBS/SiO_2 and PP/SEBS/$CaCO_3$). On the contrary, the stress triaxiality of the blend (75/22/3 vol %) was smaller than that of the blend (73/21/6 vol %) in both blends. These finite element results indicated that the blend (75/22/3 vol %) was more ductile than the blend (73/21/6 vol %).

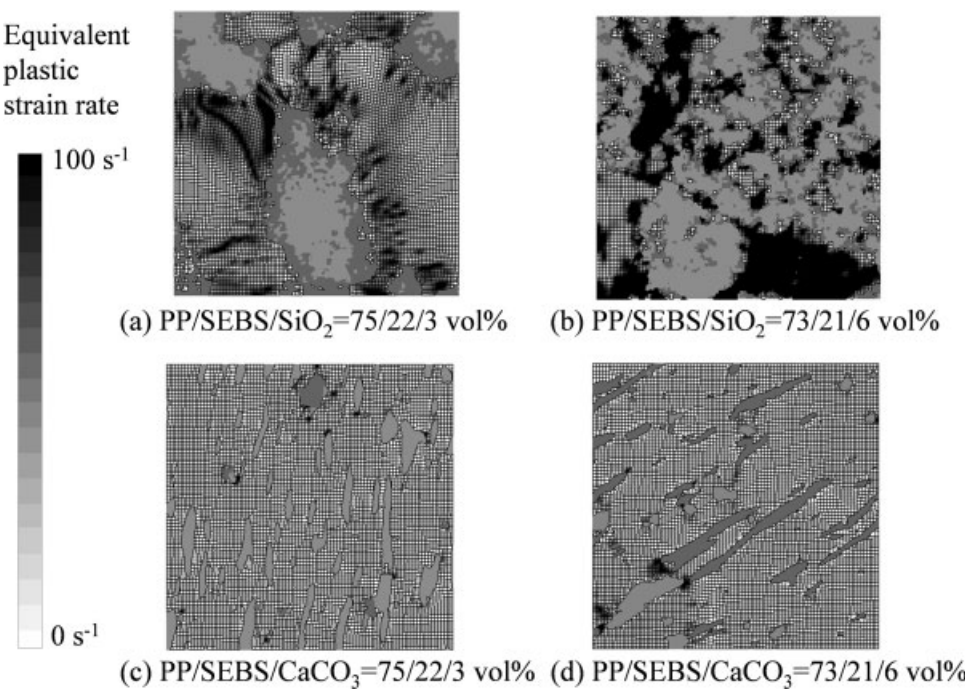

Figure 17 Simulated equivalent plastic strain rate distributions of PP/SEBS/SiO_2 ($CaCO_3$) blends at $\varepsilon_x = \varepsilon_y = 0.1$.

Figure 17 shows the equivalent plastic strain rate distribution of PP/SEBS/SiO_2 ($CaCO_3$) blends at $\varepsilon_x = \varepsilon_y = 0.1$. In the blends (PP/SEBS/SiO_2), it is observed that the SiO_2 nanoparticles around SEBS particles increased the local strain rate of the PP matrix compared with the blend (PP/SEBS/$CaCO_3$). On the contrary, the local strain rate was not enhanced in the blends (PP/SEBS/$CaCO_3$). Thus, it is considered that the apparent elastic modulus of the blends (PP/SEBS/SiO_2) should increase at the nominal strain rate above 50 s^{-1} because the local strain rate of PP matrix would get larger. On the basis of the tensile test result, the ductile brittle transition was found at the nominal strain rate between 10 and 50 s^{-1} as shown in Figure 5. As the deformation proceeded, the SiO_2 nanoparticles around SEBS particles should get removed from the boundary between PP and SEBS particles, leading to the similar deformation mechanism as the PP/SEBS blend. On the contrary to the blend (PP/SEBS/SiO_2 = 75/22/3 vol %), the deformation mechanism mentioned above could not occur in the blend (PP/SEBS/SiO_2 = 73/21/6 vol %) because the SiO_2 aggregation size was too large to break the aggregation during the large deformation although this lager SiO_2 aggregation structure enhanced the apparent elastic modulus at the whole range of strain rates in this study.

CONCLUSIONS

The effects of two types of inorganic fillers (SiO_2 and $CaCO_3$) on the mechanical properties of PP/SEBS blend at the intermediate and high strain rates were characterized. The morphology of polymer blends was observed and the distribution sizes of the SEBS particles, SiO_2 and $CaCO_3$ were analyzed by transmission electron microscopy (TEM). Tensile tests were conducted at nominal strain rates from 3 $\times 10^{-1}$ to 10^2 s^{-1}. In addition, the microstructural FE analysis was conducted to investigate the craze growth, the stress triaxiality and the local strain rate. The followings are the conclusions of this study:

1. The apparent elastic modulus has some difference of stiffening effect by adding SiO_2 nanoparticles and $CaCO_3$ fillers. Adding SiO_2 nanoparticles by 3 vol % increased the apparent elastic modulus of the blend (PP/SEBS = 75/25 vol %) by 60% at the high strain rate while SiO_2 nanoparticles did not enhance the stiffness at the low strain rate. This is because the SiO_2 nanoparticles around SEBS particles made the local strain rate larger in the PP matrix.
2. The yield stress is weak dependency of morphology. The strain rate dependency of yield stress was smaller than that of apparent elastic modulus.
3. The absorbed strain energy has strong dependency of the location of SiO_2 nanoparticle or $CaCO_3$ fillers and SEBS particle in the morphology. During the deformation process, SiO_2 nanoparticles located around SEBS particles would get removed from the boundary between PP and SEBS, leading to 20% increased ductility compared with that of the blend (PP/SEBS = 75/25 vol %).
4. It is considered that such morphology that inorganic nanoparticles are located around SEBS particles can prevent the brittle fracture while the increased local strain rate can enhance the elastic modulus of the blend at the high strain rate.

On the basis of the results of this study, the location and size of inorganic nanoparticles are the most important parameters to increase the elastic modulus without decreasing the material ductility of the blend at both low and high strain rates. Therefore, for the next step of the present study, it would be necessary to study further the effect of the location and size of SiO_2 nanoparticles or smaller-size $CaCO_3$ fillers on the elastic modulus and the ductility.

The authors acknowledge Center for Advanced Materials Analysis, Tokyo Institute of Technology for helping the TEM observation.

References

1. Pukanszky, B.; Tudos, F.; Kolarik, J.; Lednicky, F. Polym Comp 1990, 11, 98.
2. Jancar, J.; Dibenedetto, A. T. J Mater Sci 1994, 29, 4651.
3. Gubbels, F.; Ferome, R.; Teyssie, Ph.; Vanlathem, E.; Dletour, R.; Calderone, A.; Parente, V.; Bredas, J. L. Macromolecules 1994, 27, 1972.
4. Gubbels, F.; Blacher, S.; Vanlathem, E.; Jerome, R.; Deltour, R.; Brouers, F.; Teyssie, Ph. Macromolecules 1995, 28, 1559.
5. Shanks, R. A.; Long, Y. Polym Network Blend 1997, 7, 87.
6. Gubbels, F.; Jerome, R.; Vanlathem, E.; Deltour, R.; Blacher, S.; Brouers, F. Chem Mater 1998, 10, 1227.
7. Hammer, C. O.; Maurer, F. H. J.; Molnar, S.; Pukanszky, B. J Mater Sci 1999, 34, 5911.
8. Premphet, K.; Horanont, P. Polymer 2000, 41, 9283.
9. Gand, D. J.; Gao, W. J.; Song, C. S.; Wang, Z. J Mater Lett 2001, 51, 120.
10. Gonzalez, J.; Albano, C.; Ichazo, M.; Diaz, B. Eur Polym J 2002, 38, 2465.
11. Thongruang, W.; Spontak, R. J.; Balik, C. M. Polymer 2002, 43, 3717.
12. Fisher, I.; Siegmann, A.; Narkis, M. Polym Compos 2002, 23, 34.
13. Sahnoune, F.; Lopez Cuesta, J. M.; Crespy, A. Polym Eng Sci B 2003, 43, 647.
14. Zhang, L.; Li, C. Z.; Huang, R. J Polym Sci 2005, 43, 1113.
15. Sung, Y. T.; Han, M. S.; Song, H. K.; Jung, J. W.; Lee, H. S.; Kum, C. K.; Joo, J.; Kim, W. N. Polymer 2006, 47, 4434.
16. Chang, S. Q.; Xie, T. X.; Yang, G. S. J Appl Polym Sci 2006, 102, 5184.

17. Xavier, S. F.; Schultz, J. M.; Friedrich, K. J Mater Sci 1990, 24, 2411.
18. Fekete, E.; Molnar, Sz.; Kim, G.-M.; Michler, G. H.; Pukanszky, B. J Macromol Sci B 1999, 38, 885.
19. Chan, C.-M.; Wu, J.; Li, J.-X.; Cheung, Y.-K. Polymer 2002, 43, 2981.
20. Leong, Y. W.; Ishak, Z. A. M.; Ariffin, A. J Appl Polym Sci 2004, 91, 3327.
21. Maerinrri, F.; Ricco, T. J Mater Sci 1994, 29, 442.
22. Premphet, K.; Horanont, P. J Appl Polym Sci 2000, 76, 1929.
23. Rong, M. Z.; Zhang, M. Q.; Zheng, Y. X.; Zeng, H. M.; Walter, R.; Friedrich, K. J Mater Sci Lett 2000, 19, 1159.
24. Rong, M. Z.; Zhang, M. Q.; Zheng, Y. X.; Zeng, H. M.; Walter, R.; Friedrich, K. Polymer 2001, 42, 167.
25. Rong, M. Z.; Zhang, M. Q.; Zheng, Y. X.; Zeng, H. M.; Friedrich, K. Polymer 2001, 42, 3301.
26. Rong, M. Z.; Zhang, M. Q.; Pan, S. L.; Friedrich, K. J Appl Polym Sci 2004, 92, 1771.
27. Wu, C. L.; Zhang, M. Q.; Rong, M. Z.; Friedrich, K. Comp Sci Tech 2002, 62, 1327.
28. Lehmann, B.; Friedrich, K.; Wu, C. L.; Zhang, M. Q.; Rong, M. Z. J Mater Sci Lett 2003, 22, 1027.
29. Yang, H.; Zhang, Q.; Guo, M.; Wang, C.; Du, R. N.; Fu, Q. Polymer 2006, 47, 2106.
30. Yang, H.; Zhang, X.; Qu, C.; Li, B.; Zhang, L.; Zhang, Q.; Fu, Q. Polymer 2007, 48, 860.
31. Mae, H.; Omiya, M.; Kishimoto, K. J Solid Mech Mater Eng 2008, 2, 254.
32. Mae, H.; Omiya, M.; Kishimoto, K. J Appl Polym Sci 2008, 107, 3520.
33. Mae, H.; Omiya, M.; Kishimoto, K. J Soc Mater Sci Japan 2008, 57.
34. Mae, H.; Omiya, M.; Kishimoto, K., to appear.
35. http://www.ctcms.nist.gov/oof/
36. Murakami, D.; Kobayashi, S.; Torigaki, T.; Shizawa, K. Trans Japan Soc Mech Eng A 2002, 68, 674.
37. Murakami, D.; Kobayashi, S.; Torigaki, T.; Shizawa, K. Trans Japan Soc Mech Eng A 2002, 68, 682.
38. Kobayashi, S.; Tomii, D.; Shizawa, K. Trans Japan Soc of Mechanical Engineers A 2004, 70, 810.
39. Mae, H.; Omiya, M.; Kishimoto, K. J Solid Mech Mater Eng 2007, 1, 35.
40. Mae, H.; Omiya, M.; Kishimoto, K. J Solid Mech Mater Eng, to appear.
41. Mae, H.; Omiya, M.; Kishimoto, K. submitted.